Grassmann Registration Manifolds for Face Recognition⋆

Yui Man Lui and J. Ross Beveridge

Department of Computer Science, Colorado State University,
Fort Collins, CO 80523, USA
{lui,ross}@cs.colostate.edu

Abstract. Motivated by image perturbation and the geometry of manifolds, we present a novel method combining these two elements. First, we form a tangent space from a set of perturbed images and observe that the tangent space admits a vector space structure. Second, we embed the approximated tangent spaces on a Grassmann manifold and employ a chordal distance as the means for comparing subspaces. The matching process is accelerated using a coarse to fine strategy. Experiments on the FERET database suggest that the proposed method yields excellent results using both holistic and local features. Specifically, on the FERET *Dup*2 data set, our proposed method achieves 83.8% rank 1 recognition: to our knowledge the currently the best result among all non-trained methods. Evidence is also presented that peak recognition performance is achieved using roughly 100 distinct perturbed images.

1 Introduction

The use of manifolds has received great attention in recent years. This is because manifolds capture the image variability and provide more information than a single image. There are two main schools of thought for making use of manifolds. The first is to learn the structure of manifolds whereas the other is to model the manifold directly.

Many manifold learning techniques like ISOMAP [1] and LLE [2] attempt to unfold the curved manifold onto a flat space. These manifold learning techniques need a large amount of training data and dense sampling on a manifold. Such rich training data may not be available in some real-world applications.

Another school of thought is to model the image manifold directly. Image perturbation that synthesizes a single image to a set of registration images has been employed to model nonlinear image manifolds [3] [4] [5] [6]. The manifold distances are derived by matching spanning sets, for example the tangent distance [3] and the joint manifold distance [4]. However, these methods only consider the best match between two spanning sets and ignore the curved geometry of manifolds, and the distance metric remains in Euclidean spaces.

This paper formally introduces the concept of the Grassmann registration manifold and demonstrates its utility in the context of face recognition. We construct a tangent space from a set of perturbed images. The structure of the approximated tangent space is essentially a vector space. Therefore, rather than proceeding on an unknown image manifold, we embed the approximated tangent space on a Grassmann manifold where each element on this manifold represents a subspace. The key aspect of this embedding is the use of a geodesic distance which is well defined on Grassmann manifolds, thus the underlying geometry is exercised.

Our proposed method assumes local linearity and selects k nearest neighbors from a registration manifold to form a tangent space. The tangent space is then approximated and embedded on a Grassmann manifold. A chordal distance is used to compute the distance between vector spaces. To ease the illumination effect, histogram equalization followed by a Gabor filter is applied. We employ a holistic image as a primary mode as well as an ensemble of classifiers using both holistic and local features.

Comparisons to seven well-known and recent algorithms on the FERET database suggest our algorithm is competitive with the best, achieving a rank 1 recognition rate of 83.8% on the the most challenging probe set (Dup2). Only one of the seven algorithms does better at 85.0%, and unlike our method, this algorithm is a trained method. While of course training can be valuable, it introduces a set of concerns about generalization that non-trained methods avoid.

The rest of this paper is organized as follows: Related work is discussed in Section 2. Grassmann manifolds and subspace distances are reviewed in Section 3. The Grassmann registration manifolds are presented in Section 4. The image features and image preprocessing method are revealed in Section 5. The outline of our proposed algorithm is given in Section 6. The coarse and fine matching strategy is introduced in Section 7. Finally, the experimental results and conclusions are provided in Section 8 and Section 9 respectively.

2   Related Work

Image perturbation that expands a single image to an image-set has been exercised for more than a decade and proven to be be useful and effective. In this section, we summarize some of the related methods.

Simard et al. [3] considered using synthesized images to model a nonlinear manifold. Tangent planes are approximated by a first order Taylor expansion. The distance between tangent planes, called tangent distance, is then used to measure the distance between manifolds. However, the tangent distance is still defined in the Euclidean space, and the geometry of manifolds has not been examined.

Fitzgibbon and Zisserman [4] computed a joint manifold distance to cluster appearances. The manifold is captured by a mean and a set of basis vectors. Affine transformation is added to a set of spanning images to overcome geometric

deformation. This makes the measure affine resilient for appearance clustering. Although the span of a linear space is computed as a subspace distance, only the infimum between points in two subspaces is considered. As a result, the underlying geometry of manifolds remains imperceptible.

Nakayama and Kumakura [5] extracted three facial expressions (smiles, anger, and screams) using an eigenspace method. Then synthesized facial expressions are produced and added into a model as additional training data. Support vector machines were used to perform the classification.

Martínez [7] employed image perturbation to model localization errors using a single training image per class (i.e. subject). Perturbed images are utilized for learning all possible localization errors. These localization errors are modeled as a subspace by means of a mixture of Gaussians distribution for all training images such that imprecise localization can be tolerated.

Arandjelovic and Cipolla [6] modeled a face manifold as a probability distribution in video sequences. The face manifold is repopulated by a set of randomly drawn affine synthesized images. These synthesized images are augmented in the face manifold. The RANSAC algorithm is applied to remove outliers. The image data are then projected on a kernel PCA space and a symmetry version of the Kullback-Leibler divergence is exploited to compute the distance. Essentially, this method models face images on an unknown manifold.

Lui et al. [8] embedded a set of images on Grassmann manifolds and computed a geodesic distance for a subset of FRGC, version 2, experiment 4. This method achieves 15% and 40% improvements for face identification and face verification over MSM by switching to a geodesic distance. Moreover, the verification rates can be further boosted up by 50% when cohort normalization is employed in conjunction with image-set matching.

3   Grassmann Manifolds and Subspace Distances

To facilitate our discussion of Grassmann registration manifolds, we briefly describe the properties of Grassmann manifolds, canonical angles, and subspace distances. Detail descriptions on these subjects can be found in [9].

3.1   Grassmann Manifolds

A Grassmann manifold $\mathbb{G}_{n,p}$ is a set of p-dimensional linear subspaces of $\mathbb{R}^n$ (p-planes in $\mathbb{R}^n$) for $0 < p \leq n$. This Grassmann manifold has a natural quotient representation $\mathbb{G}_{n,p} = \mathbb{V}_{n,p} \ / \ \mathbb{O}_p$, where $\mathbb{V}_{n,p}$ is a Stiefel manifold (a set of $n \times p$ orthonormal matrices) and $\mathbb{O}_p$ is the orthogonal group. This representation states that two matrices belong to the same equivalence class if their columns span the same p dimensional subspace. Hence, the entire equivalence class can be represented as the subspace spanned by the columns of a given matrix $\mathcal{Y}$.

$$[\mathcal{Y}] = \{\mathcal{Y}Q_p : Q_p \in \mathbb{O}_p\} \tag{1}$$

In other words, a point on the Grassmann manifold is a linear subspace which may be specified by any arbitrary orthogonal basis.

3.2   Canonical Angles

Given two vectors x and $y \in \mathbb{R}^n$, the angle between these two vectors is defined as

$$\angle\{x,y\} = \arccos \frac{\langle x, y \rangle}{\| x \| \| y \|} \tag{2}$$

For subspaces, one can recursively define a set of angles between them which are called canonical angles, also known as principal angles [10]. Let $[\mathcal{X}]$ and $[\mathcal{Y}]$ be two subspaces in $\mathbb{R}^n$ then the canonical angles, $\angle_k\{[\mathcal{X}], [\mathcal{Y}]\}$, can be defined recursively as

$$\cos(\theta_k) = \max_{u \in [\mathcal{X}]} \max_{v \in [\mathcal{Y}]} u^T v = u_k^T v_k \tag{3}$$

subject to

$$\| u \| = \| v \| = 1, \quad u^T u_i = 0, \quad v^T v_i = 0, \quad i = 1, \ldots, k-1$$

Clearly, $\angle_k\{[\mathcal{X}], [\mathcal{Y}]\} \in [\, 0, \frac{\pi}{2}\,]$, and Θ is a vector of all canonical angles.

3.3   Subspace Distances

Since the Grassmannian space is curved, the shortest distance between points on this space is geodesic. Wong [11] shows that the geodesic distance is defined using a set of canonical angles shown as

$$d_g(\mathcal{X}, \mathcal{Y}) = \| \Theta \|_2 \tag{4}$$

However, this distance is not differentiable everywhere. An alternative measure of geodesic distance is a chordal distance [12] defined as

$$d_c(\mathcal{X}, \mathcal{Y}) = \| \sin \theta \|_2 \tag{5}$$

The chordal distance approximates the geodesic distance when the planes are close and is differentiable everywhere. We employ $d_c(\mathcal{X}, \mathcal{Y})$ as our subspace distance metric.

4   Grassmann Registration Manifolds

4.1   Registration Manifolds Formation

Sampling and characterizing a registration manifold is the key step in our proposed approach. Given a pair of eye coordinates, we determine a set of affine parameters for geometric normalization. The affine transformation maps the

(x, y) coordinate from a source image to the (u, v) coordinate of a normalized image. The transformation can be written as follows:

$$
\begin{pmatrix} u \\ v \\ w \end{pmatrix} = \begin{pmatrix} \cos(\theta) & -\sin(\theta) & dx \\ \sin(\theta) & \cos(\theta) & dy \\ 0 & 0 & 1 \end{pmatrix} \begin{pmatrix} 1 & q & 0 \\ 0 & 1 & 0 \\ 0 & 0 & 1 \end{pmatrix} \begin{pmatrix} 1+s_x & 0 & 0 \\ 0 & 1+s_y & 0 \\ 0 & 0 & 1 \end{pmatrix} \begin{pmatrix} x \\ y \\ z \end{pmatrix} \tag{6}
$$

where the first matrix describes rotation and translation, the second matrix represents skew, and the third matrix denotes scaling. These transformed coordinates can be re-written more compactly as:

$$
\begin{pmatrix} u \\ v \end{pmatrix} = \begin{pmatrix} p_1 & p_3 & p_5 \\ p_2 & p_4 & p_6 \end{pmatrix} \begin{pmatrix} x \\ y \\ 1 \end{pmatrix} \tag{7}
$$

Equation 7 reveals that there are six control parameters for the affine transformation. In this paper, a set of registration images are sampled by perturbing these six affine parameters as shown in Equation 8.

$$
\begin{pmatrix} u \\ v \end{pmatrix} = \begin{pmatrix} p_1 + \Delta p_1 & p_3 + \Delta p_3 & p_5 + \Delta p_5 \\ p_2 + \Delta p_2 & p_4 + \Delta p_4 & p_6 + \Delta p_6 \end{pmatrix} \begin{pmatrix} x \\ y \\ 1 \end{pmatrix} \tag{8}
$$

Specifically, we perturb the initial affine parameters with Δp in a $\pm$ range, such that we synthesize 3^6 (729) perturbed images. These 729 images reside on an affine registration manifold $\mathcal{M}$. In our experiments, we employ bilinear interpolation for sampling the registration manifold, and set Δp_1, Δp_2, Δp_3, and Δp_4 as {-0.03, 0, 0.03}, and Δp_5 and Δp_6 as {-3, 0, 3}. An example of registration images is given in Fig. 1.

Fig. 1. Examples of registration images

4.2   Grassmann Registration Manifolds Formation

The affine registration manifold has a nonlinear structure [3]. One way to utilize the sampled registration manifold is to assume local linearity and explore its tangent space. By the mean value theorem [13], we can approximate a tangent vector using a nearby secant. A collection of these approximated tangent vectors at a point $x \in \mathbb{R}^n$ forms a tangent space. The logical choice for the base point x

is the canonical sampled image ($\Delta p_i = 0$ in Equation 8) illustrated by the center image in Fig. 1.

The selected base point x is assumed to be an interior point that has a neighborhood homeomorphic to an open ball. Then, given k nearest neighbors $\{x_1^*, x_2^*, \ldots, x_k^*\}$ where $x_i^* \in \mathcal{M}$, a tangent space centered at x on a registration manifold $\mathcal{M}$ may be represented as:

$$T_x\mathcal{M}: \quad x + \text{span}\{x - x_1^*, x - x_2^*, \ldots, x - x_k^*\} \tag{9}$$

where $\{x - x_1^*, x - x_2^*, \ldots, x - x_k^*\}$ are the approximated tangent vectors around x. This tangent space $T_x\mathcal{M}$ has a vector space structure and any point on this tangent space can be reconstructed as:

$$x + \sum_{i=1}^{k} \alpha_i(x - x_i^*) \tag{10}$$

The k nearest neighbors define the tangent basis. Because we assume local linearity about x, the k nearest neighbors are defined using an Euclidean distance:

$$x_k^* = x_{k-1}^* \bigcup \underset{x_j \notin x_{k-1}^*}{\operatorname{argmin}} \| x - x_j \|_2^2 \tag{11}$$

where $x_0^* = \{\}$. Although we apply the same image perturbation to generate each sampled image, the k nearest neighbors for different face images are usually different. This is because changing the face image may change the relative Euclidean distances between different perturbed images.

Recall that a Grassmann manifold $\mathbb{G}_{n,p}$ is a set of p-dimensional linear subspaces of $\mathbb{R}^n$. Because a tangent space admits a vector space structure, and the approximated tangent vectors are the bases spanning the subspace, we use these tangent vectors to embed a linear subspace on a Grassmann manifold. The benefits of embedding a subspace on a Grassmann manifold are that its properties and distance metrics are well studied. Since we embed the registration manifold on a Grassmann manifold, we call the resulting manifold the Grassmann Registration Manifold (GRM).

Selecting the number of nearest neighbors to approximate the tangent space has significant implications. At the extreme low end, $k = 1$, minimizing the chordal distance equates to maximizing the correlation between pairs of images (Equation 2). At the other extreme, taking hundreds or thousands of samples is not only computationally burdensome; at some point the local linearity assumption is stretched beyond the breaking point. The effect of different choices for k on the FERET $Dup2$ data set is shown in Fig. 2. As Fig. 2 depicts, the rank 1 recognition rate starts to decrease when k is larger than 128. In our experiments, we choose $k = 100$. As Fig. 2 suggests, any value around 100 can be expected to perform well.
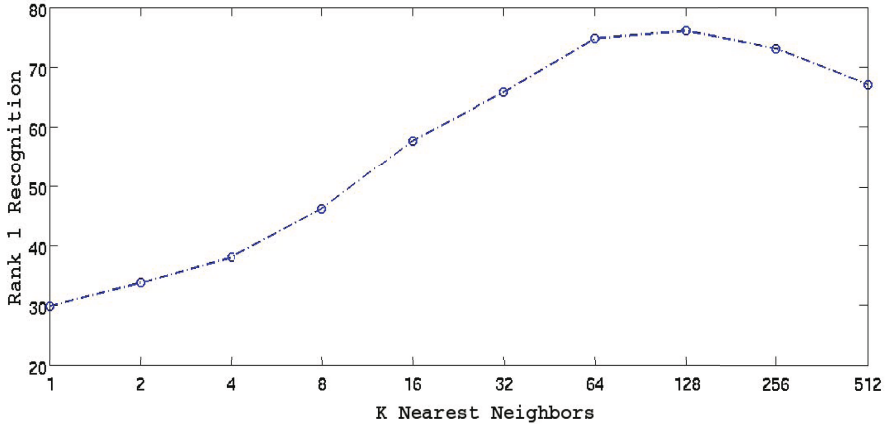
Fig. 2. The effect of K nearest neighbors

5   Image Features and Image Preprocessing

A holistic image is regarded as the whole face whereas local features can be divided into local components and local regions [14]. Local components are typically an interesting part of the face, for example an eye. Local regions are derived from regular sampling patterns, for example a grid laid over the face. In this paper, we employ a holistic image, local components, and local regions for face recognition. We choose the local components as the upper face, lower face, eyes, left eye and right eye. Local regions are 3×3 and 5×5 facial windows.[1] Examples of a holistic face, local components, and local regions are given in Fig. 3.

Fig. 3. Examples of a holistic face, local components, and local regions

For each probe and gallery image, the 729 registration images are sampled using eye coordinates provided with the data along with the perturbation process

---

[1] Since most of the lower left and lower right regions are covered by a mask in the 5 $\times$ 5 facial window, we eliminate these two regions from our feature set.

described previously. An elliptical mask is applied to remove the background. At this point the local regions are left alone while histogram equalization and a Gabor filter [15] are applied to the holistic image and local components. Treating local regions differently from local components makes classifiers based upon local regions and local components more independent. The specific DC-free Gabor filter is defined as follows:

$$\psi_{u,v}(z) = \frac{\parallel k_{u,v} \parallel^2}{\sigma^2} e^{(-\parallel k_{u,v}\parallel^2 \parallel z\parallel^2/2\sigma^2)} \left[e^{ik_{u,v}z} - e^{-\sigma^2/2} \right], \quad k_{u,v} = \frac{k_c}{f^v} e^{i\phi_u} \quad (12)$$

where u and v are the control parameters for orientations and scales, respectively, and z is the position. In our experiments, we set the $f = \sqrt{2}$, $k_c = \frac{4\pi}{5}$, $\sigma = \frac{3\pi}{2}$, $v = 0$, and $\phi_u = 0$.

6   The Grassmann Registration Manifold Algorithm

Putting all things together, the outline of the proposed Grassmann Registration Manifold (GRM) algorithm is given as follows:

– Use eye coordinates to determine the initial affine registration parameters $p_1, \ldots, p_6$ for each image. (Equation 7)
– Sample the affine registration manifold by perturbing the affine parameters (Equation 8)
– Compute the k nearest neighbors $\{x_1^*, x_2^*, \ldots, x_k^*\}$ from the registration manifold (Equation 11)
– (Optional) Apply histogram equalization and a Gabor filter (Equation 12)
– Construct the tangent space (Equation 9)
– Embed the approximated tangent space and compute canonical angles (Equation 3)
– Compute the subspace distance (Equation 5)

7   Coarse to Fine Matching Strategy

Initial studies of cumulative match curves indicate that 95% of the correct identifications are included in the top 10% of gallery candidates using just holistic image matching and $k = 16$, i.e. 16 registration manifold samples. Consequently, considerable time can be saved with a coarse to fine matching strategy as depicted in Fig. 4. The approach is coarse to fine not in the traditional sense of reduced image resolution, but instead in the sense of a reduced number of gallery candidates.

   Note that each probe image has its own gallery candidates. Once the 16 sample matching is completed, the top 10% gallery candidates are passed to the 32 sample level. In the 32 sample level, only these 10% gallery candidates will

be searched. Similarly, the top 5% of the gallery candidates are propagated to the 100 sample level and are examined. We can further propagate the top 5% gallery candidates to all local features. This coarse to fine strategy speeds up the matching process by roughly a factor of 800, (20×40).[2]
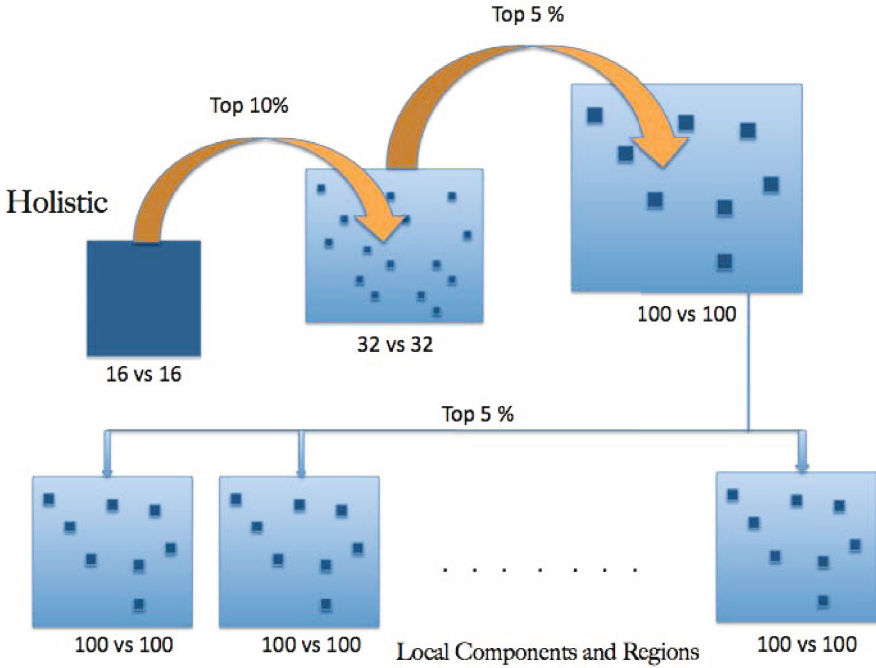

Fig. 4. The proposed coarse to fine matching strategy

8 Experiments

8.1 Data Collection

The performance of our proposed algorithm is compared to well-known algorithms on the FERET database [16]. The frontal view imagery of the FERET database is divided into 5 categories: Fa, Fb, Fc, $Dup1$, and $Dup2$, containing 1,196, 1,195, 194, 722, and 234 faces, respectively. Both Fa and Fb are taken in the same day with the same illumination condition but with different facial expressions. Fc is taken at the same day as Fa but with different illumination condition. $Dup1$ is acquired on different days from Fa. $Dup2$ is acquired at least one year apart from Fa. Following the FERET protocol, Fa is always the gallery and Fb, Fc, $Dup1$, and $Dup2$ are used as probe sets.

---

[2] 5% candidates and 40 features.

8.2   Prior Art on the FERET Database

The Elastic Bunch Graph Matching (EBGM) algorithm [17] was one of the top algorithms for the FERET database for more than half of a decade until the Local Binary Pattern (LBP) [18] was introduced. Since then, many LBP-like algorithms have been reported and continue to push the performance envelope for FERET. Zhang et al. [19] applied Gabor filters to extract local patterns and encoded them as phase-quadrant and XOR patterns. Tan and Triggs [20] proposed to combine Gabor and LBP features, and projected it on a discriminant space using kernel discriminative common vectors. Zou et al. [14] used a large set, $4,172$, of Gabor jets and achieved excellent results.

Liu et al. [21] create 9 images by horizontally and vertically shifting samples (left/right and up/down). The authors view these images as the basis for linear spatial filters because the 9 translated images make up a filter mask. Subsequently, the subspace distance between local patches is computed and the aggregated score is used for final classification. We include this algorithm in our comparison because it involves subspaces defined by different registration samples, and is thus related to our own work. However, Liu et al. only present their approach in the context of linear spatial filters, whereas we consider the underlying geometrical interpretation. In such, we make use of local linearity and do not choose the same image set all the times.

Table 1 summarizes the results of the above algorithms and two variants of our proposed method for the FERET database. The rightmost column indicates whether an algorithm requires training.

Table 1. Rank 1 recognition rate on the FERET database

Methods	Fb	Fc	Dup1	Dup2	Trained
EBGM [17]	95.0	82.0	59.0	52.0	Yes
Gabor-LBP-KDCV [20]	98.0	98.0	90.0	85.0	Yes
Weighted LBP [18]	97.0	79.0	66.0	64.0	Yes
Non-Weighted LBP [18]	93.0	51.0	61.0	50.0	No
HGPP [19]	97.6	98.9	77.7	76.1	No
GaborJets [14]	99.5	99.5	85.0	79.5	No
SIS [21]	91.0	90.0	68.0	68.0	No
GRM-Holistic	94.1	92.8	70.8	76.9	No
GRM-Local	97.5	97.9	79.5	83.8	No

8.3   Results with the Holistic Feature

Using the entire face image, our **GRM-Holistic** achieves 94.1%, 92.8%, 70.8% and 76.9% rank 1 recognition for Fb, Fc, $Dup1$, and $Dup2$, respectively. These results already outperform half of the top algorithms shown in Table 1. Specifically, the proposed **GRM-Holistic** ranks second among all non-trained algorithms and third among all algorithms for $Dup2$, the probe set for which most
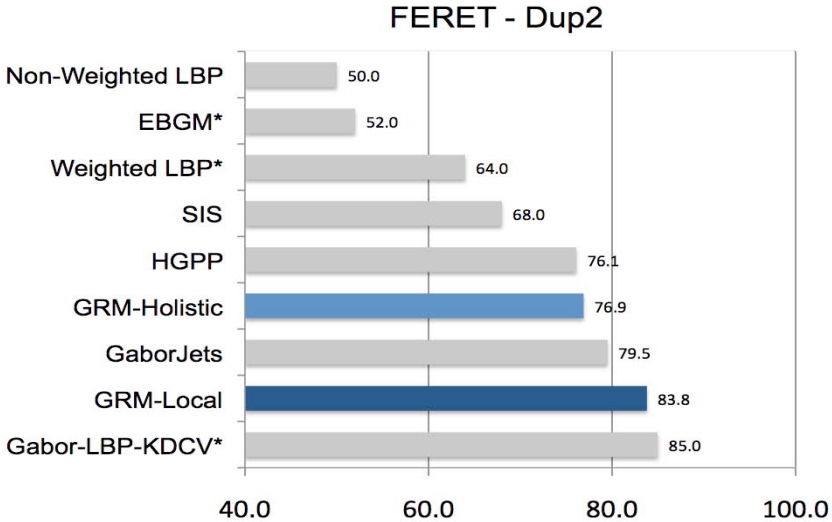
Fig. 5. Rank 1 recognition rate on the FERET database for the selected algorithms (Non-Weighted LBP [18], EBGM [17], Weighted LBP [18], SIS [21], HGPP [19], Gabor-Jets [14], and Gabor-LBP-KDCV [20]) where * indicates trained methods

algorithms have the greatest difficulty. To better visualize the ranking for $Dup2$, the results are shown from worst to best in Fig. 5.

It is worth to mention the variability associated with these rank 1 recognition rates. Assuming a binomial model [22] for rank 1 identification success/failure, a 95% confidence interval for the rank 1 recognition rate is about ± 0.05 for the FERET $Dup2$ results.

8.4   Results with Holistic + Local Features

While there is general agreement that peak performance is typically achieved using local features, Section 5 described the local features we have chosen. Fig. 6 shows the rank 1 recognition rates achieved when a GRM algorithm is constructed using each individual feature.

Neither space allows us to identify each feature, nor is it actually that important. What is important is first to note that the left most column in Fig. 6 is the holistic image as a feature, and it is consistently one of the best individual features. Hence, we can dismiss any thought that a single local feature consistently does much better than the whole image. Second, there is a fair amount of apparently random variation between features and between probe sets.

More specifically, a careful study of Fig. 6 reveals that no single local feature consistently ranks in the top 3 for all data sets. Consequently, the strength of using local features comes from the combination of independent decisions boosting recognition performance [23]. A good example is our $Dup1$ results shown in
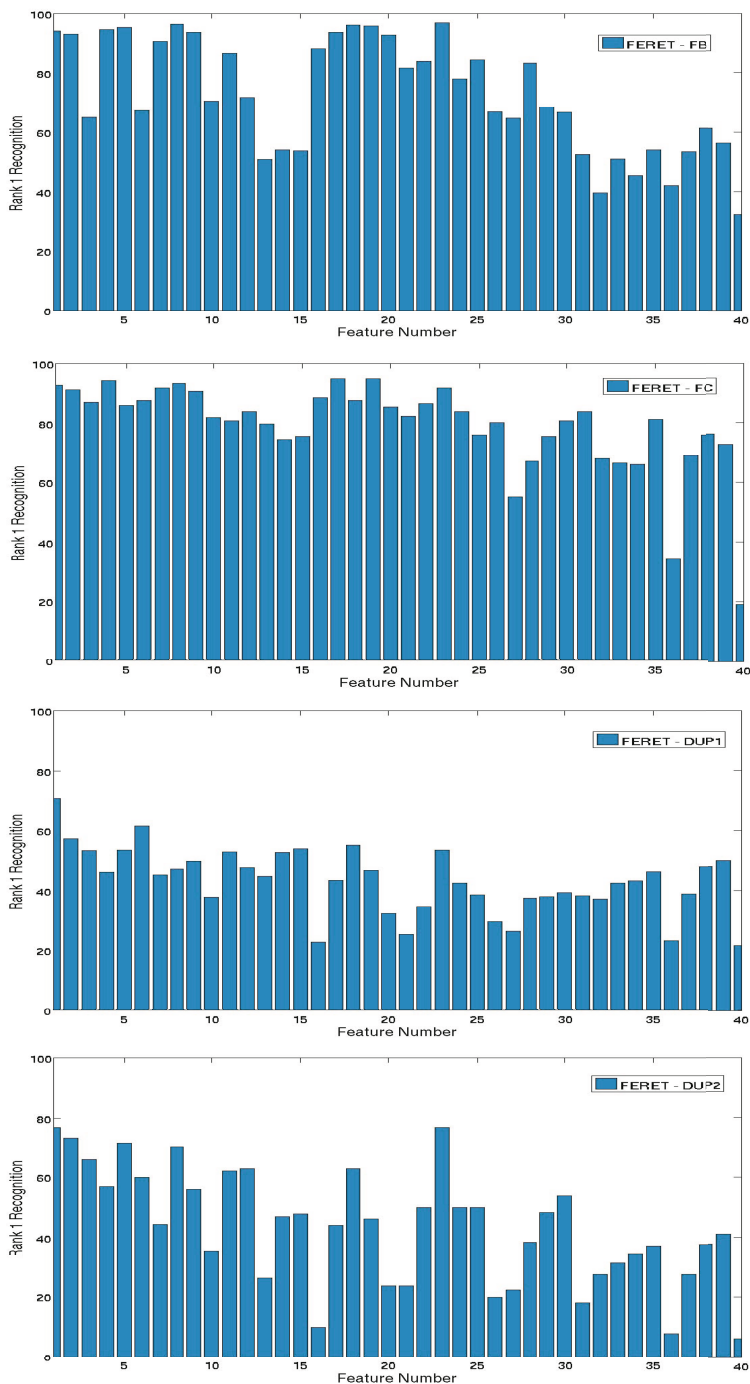
Fig. 6. Recognition rate for individual feature: The first row is Fb, the second row is Fc, the third row is Dup1 and the last row is Dup2

Fig. 6. In this paper, we use the majority voting rule [23] to combine all the feature outcomes.

Using the whole image plus local features, the **GRM-Local** algorithm achieves 97.5%, 97.9%, 79.5% and 83.8% rank 1 recognition for Fb, Fc, $Dup1$, and $Dup2$, respectively. The 83.8% rank 1 recognition for $Dup2$ is the best result for all non-trained algorithms and second among all algorithms depicted in Fig. 5.

9   Conclusions

A novel method (GRM) that embeds registration images on a Grassmann manifold is presented. We demonstrate that the underlying geometry is an important characteristic and proper utilization of this attribute enhances recognition results in the context of face recognition. Unlike many manifold learning algorithms, our proposed method does not require dense samples or training data. Therefore, our proposed method is more generic. Empirical evidence suggests that approximately 100 local samples from the affine registration manifold optimizes recognition performance. A coarse to fine matching strategy is introduced for fast computation.

A relatively simple holistic image version of our proposed GRM algorithm does very well on FERET tests, and introduction of local features further boosts recognition performance. Specifically, among all the non-trained algorithms considered, we achieve the best results of the FERET $Dup2$ data set.

Introducing the Grassmann registration manifold and associated algorithm further promotes a general trend of research into image manifolds. Our future work will focus in further exploring the question of how best to locally sample the affine registration manifold.

Acknowledgements

References

1. Tenenbaum, J., de Silva, V., Langford, J.: A global geometric framework for non-linear dimensionality reduction. Science, 2319–2323 (2000)
2. Roweis, S., Saul, L.: Nonlinear dimensionality reduction by locally linear embedding. Science, 2323–2326 (2000)
3. Simard, P., Cun, Y.L., Denker, J.: Efficient pattern recognition using a new transformation distance. Advances in Neural Information Processing System 5, 50–58 (1992)
4. Fitzgibbon, A., Zisserman, A.: Joint manifold distance: a new approach to appearance based clustering. In: IEEE Proc. Computer Vision and Pattern Recognition, Wisconsin (2003)

5. Nakayama, M., Kumakura, T.: Face identification performance using facial expressions as perturbation. In: Duch, W., Kacprzyk, J., Oja, E., Zadrożny, S. (eds.) ICANN 2005. LNCS, vol. 3696, pp. 557–562. Springer, Heidelberg (2005)
6. Arandjelovic, O., Cipolla, R.: An information-theoretic approach to face recognition from face motion manifolds. Image and Vision Computing 24(6), 639–647 (2006)
7. Martinez, A.: Recognizing imprecisely localized, partially occluded, and expression variant faces from a single sample per class. IEEE Transactions on Pattern Analysis and Machine Intelligence 24(6), 748–763 (2002)
8. Lui, Y.M., Beveridge, J.R., Draper, B.A., Kirby, M.: Image-set matching using a geodesic distance and cohort normalization. In: IEEE International Conference on Automatic Face and Gesture Recognition, Amsterdam, The Netherlands (2008)
9. Edelman, A., Arias, R., Smith, S.: The geometry of algorithms with orthogonal constraints. SIAM J. Matrix Anal. Appl. (2), 303–353 (1999)
10. Hotelling, H.: Relations between two sets of variants. Biometrika 28, 321–377 (1936)
11. Wong, Y.C.: Differential geometry of grassmann manifolds. Proc. Nat. Acad. Sci. 47, 589–594 (1967)
12. Conway, J., Hardin, R., Sloane, N.: Packing lines, planes, etc.: Packings in grassmannian spaces. Experimental Mathematics 5(2), 139–159 (1996)
13. Simon, A.: Calculus with analytic geometry. Scott, Foresman and Company (1982)
14. Zou, J., Ji, Q., Nagy, G.: A comparative study of local matching approach for face recognition. IEEE Transactions on Image Processing 16, 2617–2628 (2007)
15. Lades, M., Vorbruggen, J.C., Buhmann, J., Lange, J., von der Malsburg, C., Wurtz, R.P., Konen, W.: Distortion invariant object recognition in the dynamic link architecture. IEEE Transactions on Computers 42(3), 300–311 (1993)
16. Phillips, P., Moon, H., Rizvi, S., Rauss, P.: The feret evaluation methodology for face recognition algorithms. IEEE Transactions on Pattern Analysis and Machine Intelligence 22(10), 1090–1104 (2000)
17. Wiskott, L., Fellous, J.M., Kruger, N., Malsburg, C.: Face recognition by elastic bunch graph matching. IEEE Transactions on Pattern Analysis and Machine Intelligence 19, 775–779 (1997)
18. Ahonen, T., Hadid, A., Pietikinen, M.: Face recognition with local binary patterns. In: European Conference on Computer Vision, Czech Republic, pp. 469–481 (2004)
19. Zhang, B., Shan, S., Chen, X., Gao, W.: Histogram of gabor phase patterns (hgpp): A novel object representation approach for face recognition. IEEE Transactions on Image Processing 16, 57–68 (2007)
20. Tan, X., Triggs, B.: Fusing gabor and lbp feature sets for kernel-based face recognition. In: IEEE International Workshop on Analysis and Modeling of Faces and Gestures, pp. 235–249 (2007)
21. Liu, J., Chen, S., Zhou, Z.H., Tan, X.: Single image subspace for face recognition. In: IEEE International Workshop on Analysis and Modeling of Faces and Gestures, pp. 205–219 (2007)
22. McNemar, Q.: Note on the sampling error of the difference between correlated proportions or percentages. Psychometrika, 153–157 (1947)
23. Lam, L., Suen, C.Y.: Application of majority voting to pattern recognition: An analysis of its behavior and performance. IEEE Transactions on Systems, Man and Cybernetics, Part A 27(5), 553–568 (1997)